Sampled-Grating DBR Laser-Based Analog Optical Transmitters

L. A. Johansson, J. T. Getty, Y. A. Akulova, G. A. Fish, and L. A. Coldren

Abstract—**Sampled-grating distributed Bragg grating (SGDBR) laser-based widely tunable optical transmitters are investigated for application in high-performance analog links. More than 45 nm tuning range, 40 dB sidemode suppression ratio, and peak relative intensity noise below −153 dB/Hz is measured. SGDBR lasers integrated with semiconductor optical amplifiers and electroabsorption modulators (EAMs) are characterized with spurious free dynamic range of 125–127 dB·Hz$^{4/5}$ over the wavelength tuning range. It is also shown how the modulation response of the EAM is affected by the optical power to limit the performance of the analog transmitter.**

Index Terms—**Distributed Bragg grating lasers, electroabsorption, integrated optoelectronics, microwave photonics, optical communications.**

I. INTRODUCTION

OPTICAL fiber provides a very low loss, high bandwidth medium for transmission of microwave signals. Current applications include cable television distribution systems, where the low loss of fiber is utilized for efficient distribution of analog video signals. Another application is antenna remoting systems, where optical fiber is used as a low-loss medium to extend the radio signal path where antenna unit size/complexity needs to be minimized and system flexibility is improved by centralization of system functions. However, cost/performance constraints of the devices performing microwave-to-optical and optical-to-microwave conversion have limited the performance and wider use of analog optical links for the transport of microwave signals. One alternative prospect is the replacement of functions such as generation, amplification, frequency conversion, and transportation of microwave signals using optoelectronic components that traditionally have been performed in the electrical domain, particularly at higher frequencies, taking advantage of the potentially ultrabroadband operating range of optical systems.

For the potential of the analog optical link to be realized, much work is needed to improve the performance of current technology to a level comparable to what can be achieved using electronics and at a comparable or lower price. Analog links currently perform well in terms of frequency response, relatively inexpensive directly modulated sources can be modulated from 0 GHz to typically 10 GHz, and external optical modulators have demonstrated the possibility of modulating from dc to above 100 GHz [1]. Optical links with RF gain below 1 GHz [2], [3], low noise figure (2.3 dB at 130 MHz) [4], and high dynamic range (132 dB·Hz$^{4/5}$) [5] have also been demonstrated. However, no link has been demonstrated combining good performance in all of these areas, particularly obtaining good broadband gain/noise figure performance at higher frequencies.

In this paper, we investigate the performance of an integrated photonic transmitter module based on a monolithically integrated InP chip comprising a sampled-grating distributed Bragg grating (SGDBR) laser, a semiconductor optical amplifier (SOA), and an electroabsorption modulator (EAM) for high-performance analog optical link applications. Current efforts investigating various technologies that can be used for improving the performance of the transmitters are also summarized in this paper, particularly toward the goal of increasing the RF-to-optical conversion efficiency of the device, a prerequisite for both low link loss and low link noise figure.

This paper is structured as follows. In Section II, a brief overview of the structure and composition of the devices applied as analog transmitters is presented. In Section III, the relative intensity noise (RIN) performance of the integrated SGDBR-SOA-EAM device is shown. The direct modulation performance of the lasers is investigated in Section IV. A comprehensive investigation into the modulation response of the integrated electroabsorption modulator is presented in Section V. Finally, the transmitter is applied to a simple link demonstration, described in Section VI, before conclusions are given in Section VII.

II. DEVICE

The device used for most of the work described within this paper consists of an SGDBR laser, an SOA, and an EA modulator, all integrated on the same InP chip, as illustrated in Fig. 1. Further details regarding this type of device can be found in [6]. The SGDBR laser includes gain and phase sections positioned between two "sampled grating" distributed reflectors, sampled at different periods such that only one of their multiple reflection peaks can coincide at a time [7]. Introducing a small index change in one mirror relative to the other causes adjacent reflectivity maxima to come into alignment, shifting the lasing wavelength a large amount for small index change. Continuous tuning between the reflectivity maxima is obtained by tuning both mirrors, resulting in a quasi-continuous tuning range greater than 45 nm. Biasing of the phase section fine-tunes the effective Fabry–Perot cavity mode into alignment with the maximum reflectivity of the mirrors. The integrated SOA

L. A. Johansson, J. T. Getty, and L. A. Coldren are with the Department of Electrical and Computer Engineering, University of California, Santa Barbara, CA 93106 USA (e-mail: leif@ece.ucsb.edu).

Y. A. Akulova and G. A. Fish are with Agility Communications, Inc., Santa Barbara, CA 93117 USA.

compensates for on-state modulator loss, and for cavity losses caused by free carrier absorption in the tuning sections, and allows wavelength-independent power leveling. More than 10 mW output power, narrower than 2 MHz linewidth, and greater than 40 dB sidemode suppression ratio has been achieved over a wavelength tuning range greater than 40 nm [6]. Typical operation conditions for 10 mW continuous wave (CW) are $I_{gain} = 150$ mA, I_{FM}, and I_{RM} below 27 and 43 mA, respectively, and I_{SOA} below 150 mA.

The integration of the laser and SOA active regions with the tuning and modulator sections of the device has been accomplished by using an offset quantum-well structure [8]. In this integration technology, the active region of the modulator uses the same bulk quaternary waveguide as the tuning sections of the laser. The Franz–Keldysh effect in the bulk waveguide material provides for larger spectral bandwidth as compared to the quantum-confined Stark effect, as illustrated by Fig. 2. The composition of the bulk waveguide can be optimized to achieve high tuning efficiency for the laser and a target extinction ratio over the required wide spectral bandwidth for the modulator. The bulk design allows improved power handling of the device, avoiding carrier pileup problems, up to a limit determined by Joule heating of the device; this limit is an I–V product of 200 mW, with I being the EAM photocurrent and V being the absolute value of the bias voltage. The efficient coupling between the source and the modulator/detector waveguide structure makes it convenient to study high optical power effects in the EAM device.

Fig. 1. SGDBR-SOA-EAM device schematic.

Fig. 2. Measured extinction as a function of EAM reverse bias at different optical wavelengths.

III. Noise Performance

In a previous publication [9], the RIN performance of SGDBR lasers, not integrated with an SOA or an EAM, was investigated. Shot-noise limited relative noise performance of about −160 dB/Hz was measured with RIN levels lower than −160 dB/Hz at high bias current to the gain section. The RIN was found to vary over the tuning range, mainly determined by the variations of output power over the tuning range.

For the current device, the RIN is produced both in the SGDBR laser structure and in the SOA section. Fig. 3 shows the measured RIN spectra for an SGDBR laser integrated with an SOA, for different values of gain section bias. The SOA bias was fixed at 180 mA. At 200 mA, the peak RIN is lower than −153 dB/Hz. The detector shot noise contribution has been subtracted in these graphs. Fig. 4 shows the RIN for different values of bias applied to the SOA. The gain section bias was here fixed at 180 mA. The RIN improves with increasing SOA bias as expected, being minimum in the 120–140 mA range, after which increased heating slightly degrades the noise performance. The noise performance of the SOA noise is best observed at frequencies away from the laser RIN peak, particularly below a few gigahertz, where the overall noise is limited by the SOA spontaneous emission. This effect is also confirmed in Fig. 3 by the compression of RIN level around 2 GHz for gain section bias higher than 100 mA.
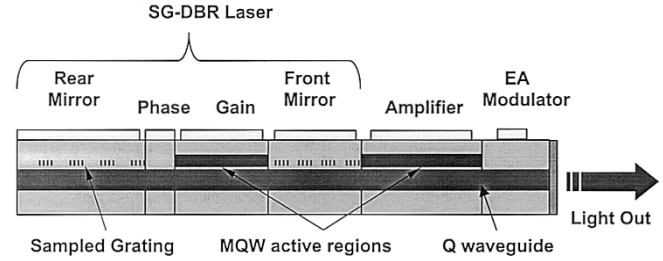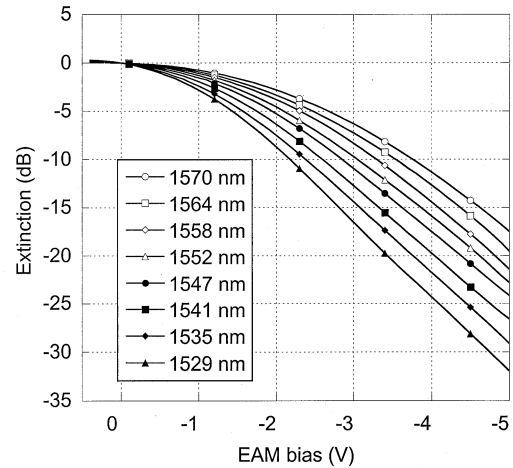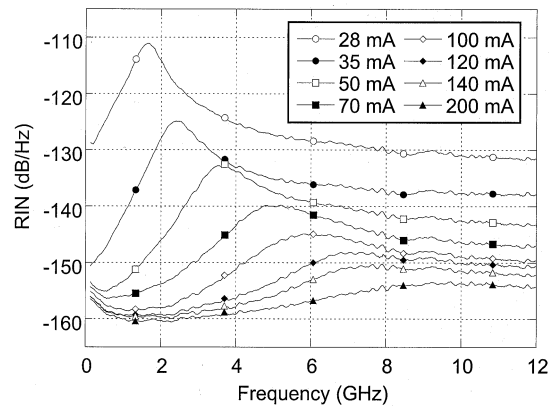

Fig. 3. Detected RIN spectra at 1552 nm for different values of gain section bias. SOA bias fixed at 180 mA.

IV. Direct Modulation Response

The modulation efficiency of a directly modulated laser is given by the current conversion efficiency η_d and optical coupling losses. For a standard semiconductor laser, the maximum possible conversion efficiency is about 0.8 W/A at 1550 nm, also referred to as 100% differential quantum efficiency (DQE). Using a typical 50-Ω terminated driver source, a serial matching load is often applied to the laser to minimize reflections. The matching load comes with a price. For a fixed output power from the source, the delivered modulation current to the laser will be nearly half of what is delivered to an unmatched laser, assuming the laser has a low input impedance. Despite these limitations,
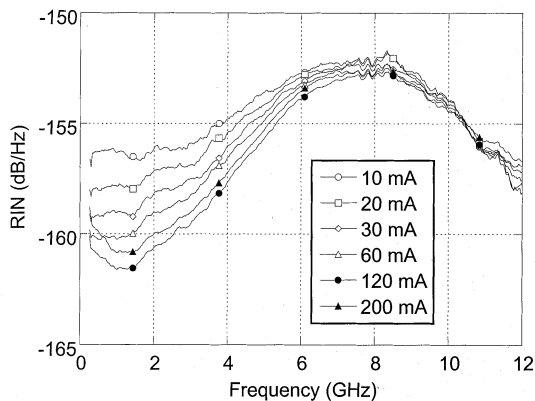
Fig. 4. Detected RIN spectra at 1552 nm for different values of SOA bias. Gain section bias fixed at 180 mA.

Fig. 5. Detected photocurrent in the reversed biased EAM as a function of gain section bias. Also shown is the "on chip" optical link gain at 1-GHz modulation frequency.

direct modulation remains one of the most efficient and simple ways of modulating a lightwave signal. Further, direct modulation has inherently a more linear response than most optical modulators. For these reasons, it is worth considering the potential improvements that are possible for directly modulated SGDBR lasers to contrast with the performance of externally modulated integrated devices.

The direct modulation response of a SGDBR laser not integrated with any SOA or EAM has previously been investigated [10], [11]. A direct modulation bandwidth up to 6 GHz was obtained. Large signal modulation without any mode-hop was also possible for 2.5-Gb/s digital application. Extinction ratios up to 10 dB were possible. Further, the spurious-free dynamic range (SFDR) of the same device has also been investigated [12]. The SFDR was measured at 112 dB · Hz$^{2/3}$ and the input power of the third-order intercept point (IIP3) was higher than 25 dBm.

Several possibilities exist to enhance the direct modulation response beyond the limit given by 100% DQE. The integrated semiconductor amplifier in the integrated SGDBR-SOA-EAM device provides gain to the modulated signal. The direct modulation efficiency is also conveniently measured by measuring the absorbed photocurrent in the EAM reverse biased for high extinction. In this manner, the direct modulation conversion efficiency can be estimated decoupled from optical coupling losses, even for a fiber-pigtailed packaged device. Fig. 5 shows the photocurrent detected by the EAM as a function of gain section bias current, the SOA being biased at a constant 180 mA. The maximum slope is on the order of 3.7 in the 30–35 mA range, indicating an equivalent DQE equal to or exceeding 370%, depending on the EAM photodetection responsivity. The higher than unity gain is attributed to the optical gain provided by the SOA. Also shown in Fig. 5 is the RF gain at 1-GHz modulation frequency. Up to 17-dB RF gain is measured between 31 and 33 mA, a result of the combination of the SOA gain and the ratio between the low input impedance of the unmatched laser and high output impedance of the EAM.

Optical amplification will improve the transmitter gain but also increase the transmitter noise to a higher degree than the slope sensitivity and can therefore only degrade the link noise figure, assuming it is not limited by receiver noise. Two methods of improving the direct modulation sensitivity
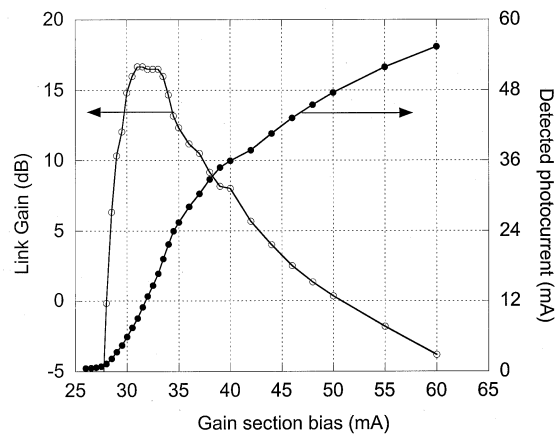
beyond 100% conversion efficiency without resorting to optical amplification that have been demonstrated are gain-levered lasers [13] and cascaded lasers [16]. The gain lever exploits nonuniform pumping of the laser to improve conversion efficiency by biasing one of two sections below threshold, such that the overall laser is biased just above threshold. It has been shown that the gain lever can improve signal-to-noise ratio (SNR) by increasing modulation sensitivity to a higher degree than increasing the RIN, improving the SNR by 7 dB [14]. A prototype gain-levered SGDBR laser has been produced, dividing the gain section of the laser into two parts: one 500 μm and one 100 μm. Enhanced modulation efficiency is obtained by pumping the two sections nonuniformly, applying the larger current density to the longer section. The increase of slope efficiency is, however, accompanied by a degradation of RIN and modulation bandwidth, which will degrade the overall performance of the analog link. One further disadvantage of the gain-levered laser is the nonlinear L–I curve [15] that will result in a low dynamic range for the analog link.

The cascaded laser approach does not inherently limit the performance of the analog link beyond that achieved using a standard laser. In this configuration, several laser gain section are biased in series, reusing the injection current to achieve more than 100% DQE. DQE of 180% has been demonstrated using a series-connected VCSEL array [16]. The problem of using discrete lasers is that the benefit of overall conversion efficiency is limited by optical coupling losses, limiting the efficiency of coupling to the optical fiber as the size of the array is increased. This limitation can be overcome by series-connecting several gain sections in a single laser structure [17], as shown in Fig. 6. Table I summarizes the CW performance of an integrated segmented Fabry–Perot laser. It is seen that as the number of sections increases while the total length of the device stays constant, the required injection current decreases linearly with the number of sections N to a DQE as high as 390% for 12 sections, while the required driving voltage increases linearly with N. The resulting input impedance therefore increases as N^2.

One of the interesting implications of Table I is the possibility of tailoring optical sources for maximizing RF power transfer

by matching link input impedance to available drivers. For example, a three-section laser is almost ideally suited for application in a standard 50-Ω system, eliminating the need for a serial matching resistor using a single-section laser, while improving the conversion efficiency by a factor of three compared to the equivalent impedance-matched single-section laser. Similarly, a larger number of sections are more suitable for high-impedance drivers, such as a high-impedance current source. Further, in contrast to gain-levered lasers, the improved conversion efficiency of these devices is not attributed by any increase in RIN, such that the improvement in SNR will be directly dependent on the increased modulation efficiency. Nor does the dynamic range of the segmented laser degrade, compared to the single-section laser. The incorporation of series-connected gain sections into a SGDBR structure has the potential of greatly enhancing the direct modulation performance of widely tunable analog optical transmitters.

Fig. 6. Schematic of segmented laser.

TABLE I
ROOM-TEMPERATURE CW CHARACTERISTICS OF THE CONTROL ($1 \times 600\,\mu$m) AND SEGMENTED LASERS

Stages & Length	Differential Efficiency	Threshold Current	Threshold Voltage	Input Impedance
12x50μm	**390%**	2.74 mA	11.3 V	471 Ω
6x100μm	218%	4.77 mA	5.8 V	117 Ω
3x200μm	126%	10.4 mA	3.0 V	**48 Ω**
1x600μm	34%	28mA	1.05 V	5.5 Ω

V. INTEGRATED MODULATOR PERFORMANCE

In terms of link performance, the use of modulator-based optical transmitters has greater potential than directly modulated lasers in many ways. In terms of bandwidth, directly modulated sources are limited. Even though 3-dB bandwidth as high as 40 GHz [18] has been demonstrated, this only applies for small-signal modulation at high bias current, where modulation sensitivity suffers. If a laser is biased just above threshold for maximum slope efficiency, both bandwidth and noise performance will suffer. Modulators are less limited by these constraints and can advantageously be used with an optical source optimized for high power, low noise operation. One disadvantage of optical modulators has traditionally been low conversion efficiency, a result of the high required driving voltage. However, the conversion efficiency is dependent on the input optical power, and given sufficient coupled optical power, the gain of an optical link using optical modulators can match, or even exceed, the gain of a directly modulated optical link, as demonstrated in [3].

A. EAM Photocurrent Effects

The integrated electroabsorption modulator used in this paper can be modeled using a simple equivalent circuit, shown in Fig. 7. R_J and $C_J(0.5$ pF) are the device junction resistance and capacitance, respectively, $R_S(7\,\Omega)$ is the device shunt resistance, $L_C(0.8$ nH) is the bondwire inductance, and $C_P(0.5$ pF) is the bonding-pad capacitance. It has previously been demonstrated that the photocurrent can be modeled as an equivalent change in junction resistance [19]. As a result of integration of the source and modulator, and the bulk design of the modulator, high optical power can be coupled to the EAM without risking damage to the device or degrading the extinction of the device. Facet damage has been shown to limit the available input optical power of waveguide p-i-n photodetectors to typically 200 mW [20], while quantum-well modulators can be saturated even at moderate optical power due to screening effects [21].

The high operating waveguide power of the device is illustrated by Fig. 8, where the complementary measurement of
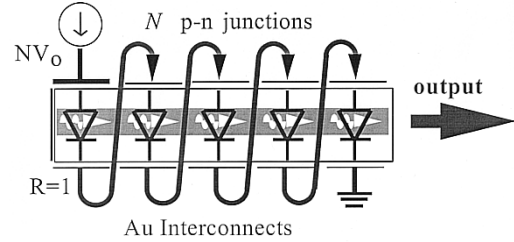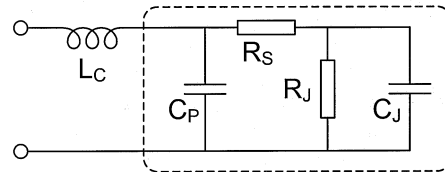

Fig. 7. EAM RF equivalent circuit model.

transmitted fiber-coupled power and absorbed photocurrent in the modulator is shown for $\lambda = 1552$ nm. In fact, the photocurrent follows an almost perfectly linear relation to the waveguide optical power to photocurrents higher than 70 mA, as we have shown in [22]. Clearly, this configuration enables study of high photocurrent effects in electroabsorption modulators. The maximum slope of the V–I curve in Fig. 8 corresponds to an equivalent device resistance of 50 Ω. This affects the response of the modulator. Fig. 9 shows S11 of the EAM in the absence of any matching circuit. For this measurement, the input optical power was regulated by adjusting the bias current of the SOA. It is seen that the reflections are strongly dependent on the input optical power, and at 115-mA SOA bias, an almost perfect 50-Ω match is achieved at lower frequencies. At higher frequencies, the reflections are also determined by the junction and pad capacitances and the bond-wire inductance. The dip in the S11 response above 10 GHz is caused by interaction between the bond-wire inductance and the capacitance at the Aluminum-Nitride substrate the device is mounted on. The equivalent device conductance can be derived from the reflections and plotted as a function of fiber-coupled optical power, shown in Fig. 10. It is seen that the conductance varies linearly with the optical power and can be as high as 0.0029 S, corresponding to only 27-Ω junction resistance in series with 7-Ω shunt resistance.
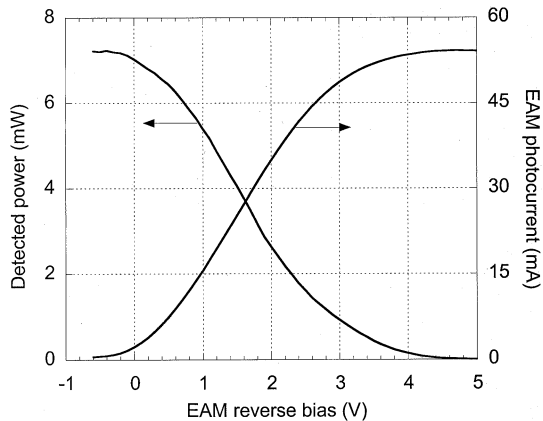
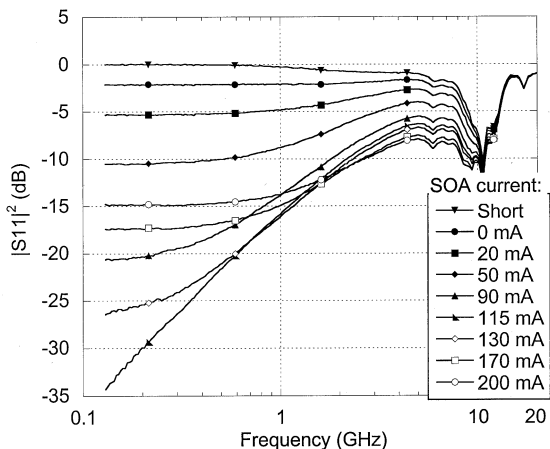Fig. 8. Fiber-coupled transmitted power and EAM photocurrent as a function of EAM reverse bias at $\lambda = 1552$ nm.
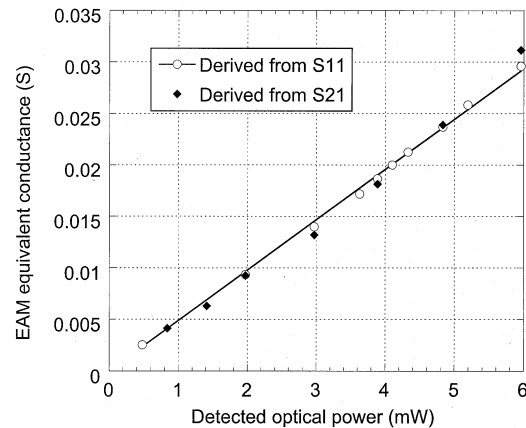

Fig. 10. Equivalent EAM conductance as a function of fiber-coupled transmitted optical power, derived from S-parameters, as a function of fiber-coupled transmitted power.
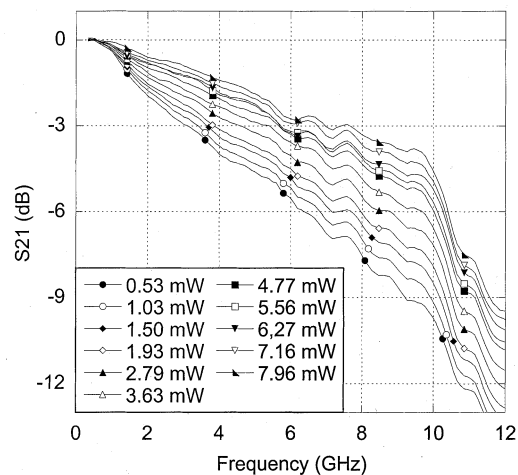

Fig. 9. EAM S11 as a function SOA bias current with 180-mA gain section current.

Fig. 11. Normalized measured EAM modulation response for different levels of fiber-coupled transmitted optical power.

B. Modulation Response

The absorbed photocurrent has dramatic effects on the modulation response of the EAM. Normally, an optical modulator is assumed to have a high input impedance; therefore the RF-to-optical conversion efficiency is determined by the voltage slope efficiency dP/dv_m and the parallel matching load, often 50 Ω, that is used for matching and providing a high bandwidth. The effects of photocurrent can be investigated by considering the modulator current slope efficiency dP/di_m. The current slope efficiency is independent of dP/dv_m, only related to the amount of absorbed optical power by the photodetection slope efficiency η_i, with a maximum value of 1.24 A/W at 1550 nm, and optical coupling losses. The slope efficiency cannot exceed the limit given by η_i, the EAM shunt resistance, and the driver output load. The photocurrent will therefore result in a compression of modulation sensitivity at lower frequencies, which in turn will affect the bandwidth.

Fig. 11 shows the normalized modulation response at different transmitted optical power levels for an unterminated EAM. The 3-dB modulation bandwidth is shown to increase from 3.3 GHz to closer to 8.0 GHz as optical power is increased from 0.53 to 7.96 mW. Deriving the device conductance from the compression of the S21 measurements, there is good agreement compared to S11 data, also shown in Fig. 10.

The EAM is currently not optimized for high bandwidth. For a 50-Ω terminated EAM, the bandwidth is about 6.5 GHz at low optical power, limited by pad and junction capacitance of about 0.5 pF each. A substantial improvement in modulator bandwidth can be obtained by minimizing pad capacitance. By reducing the EAM modulator length from 250 to 120 μm, the bandwidth increases to about 9 GHz at the price of lower modulation sensitivity.

C. Dynamic Range

The SFDR of the device is measured using two-tone modulation at 1-MHz offset. The RF power of each tone is varied between −5 to 8 dBm. Fig. 12 shows the power of the fundamental, second, and third harmonic intermodulation products as a function of EAM bias for 0 dBm modulation power of each carrier and at 0.5 GHz. Also shown in the plot is the average
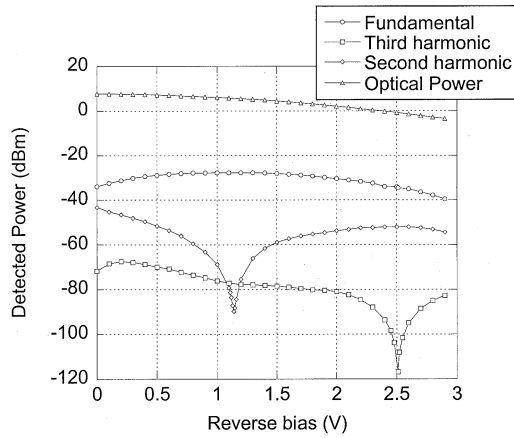
Fig. 12. Detected average optical power and RF power of fundamental and distortion products for 0-dBm modulation power.

Fig. 13. Measured power of noise floor, fundamental, and second- and third-order intermodulation products at 1552 nm for −5 to 5 dBm input RF power, 6.3-mW optical power, and −1.1-V EAM bias (where the second-order distortion products are minimized). Broadband SFDR is also shown in 1-Hz and 1-MHz bandwidth.

optical output power at $\lambda = 1545$ nm for 100 mA bias current to both the gain and SOA sections. Minimum second-order distortion is observed at the bias point where the modulation efficiency is maximum, −1.1 V at $\lambda = 1545$ nm. Minimum third-order distortion appears at −2.5 V EAM bias voltage.

For broadband linearized applications, both even-order and odd-order distortion products need to be taken into consideration. The optimum bias point for broadband operation is therefore at maximum slope efficiency, minimizing second-order distortion. Fig. 13 shows the measured dynamic range at this bias point, for both 1-Hz and 1-MHz bandwidth, limited by second- or third-order intermodulation products for 180-mA bias to both the SOA and gain sections and $\lambda = 1552$ nm. The received optical power is 6.3 mW, resulting in a noise floor at −157 dBm/Hz, limited by shot noise and laser RIN. Due to the different slope dependence of second- and third-order distortion, the SFDR is limited by third-order distortion measured in noise bandwidths down to about 200 kHz, after which second-order distortion will be limiting. The SFDR limited by second-order distortion is 97.19 dB in 1-Hz bandwidth, corresponding to 67.19 dB in 1-MHz bandwidth. The SFDR limited by third-order distortion is 106.09 dB in 1-Hz bandwidth, corresponding to 66.09 dB in 1-MHz bandwidth. Fig. 15 shows the broadband SFDR over the tuning range of the laser. The SFDR remains within a 103–107 dB · Hz$^{2/3}$ range limited by third-order intermodulation products, or 95–98 dB · Hz$^{1/2}$ range limited by second-order intermodulation products.

For suboctave linearized applications, even-order distortion products can be filtered away after detection. The EAM is therefore low biased to the bias point of minimum third-order distortion, resulting in a fifth-order slope dependence of the distortion on the input RF signal power. Fig. 14 shows the measured suboctave dynamic range for the link at this EAM bias point, for both 1-Hz and 1-MHz bandwidth. The SFDR is limited by fifth-order intermodulation products for 120-mA bias to the SOA and 180-mA to the gain section and $\lambda = 1552$ nm. The lower bias applied to the SOA is to protect the modulator from Joule heating by excessive $i - v$ product, with i being the EAM photocurrent. The received optical power is 0.96 mW, re-
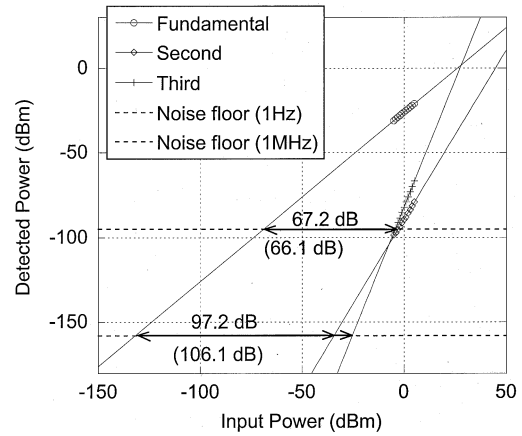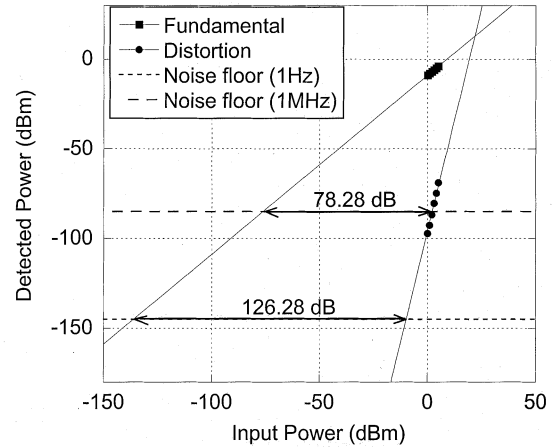

Fig. 14. Measured power of noise floor, fundamental, and second- and third-order intermodulation products at 1552 nm, for 0 to 5 dBm input RF power, 0.96-mW optical power, and −2.5-V EAM bias (where the third-order distortion products are minimized). Suboctave SFDR is also shown in 1-Hz and 1-MHz bandwidth.
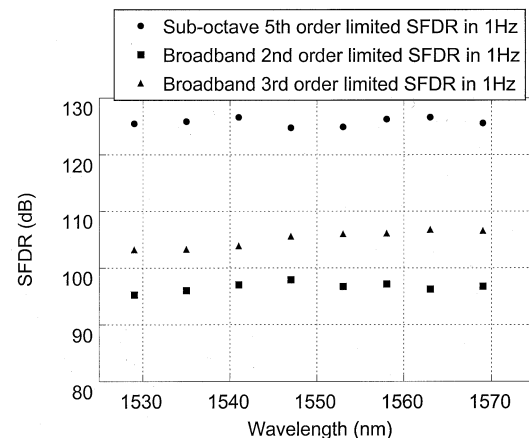

Fig. 15. Measured suboctave and broadband SFDR, left scale, normalized to 1-Hz bandwidth for different wavelengths. Suboctave SFDR limited by fifth-order intermodulation products and broadband SFDR limited by second- and third-order intermodulation products are shown.

sulting in a noise floor mainly limited by shot noise. The SFDR is 126.28 dB in 1-Hz bandwidth, corresponding to 78.28 dB in 1-MHz bandwidth. For comparison, the same performance in 1-MHz bandwidth would be offered by an SFDR of 118 dB in 1 Hz for a device limited by third-order distortion products, an important consideration when comparing, say, the performance of external modulators biased for minimum third-order distortion to that of directly modulated lasers. Fig. 15 shows the suboctave SFDR over the tuning range of the laser. The SFDR remains within a 125–127 dB $\cdot$ Hz$^{4/5}$ range, all limited by fifth-order intermodulation products.

The power of the distortion products relative to the fundamental and optimum EAM bias point for minimum distortion does not change significantly for modulation frequencies within the bandwidth of the modulator, up to 10 GHz for a 50-Ω terminated device. This is shown in Fig. 16, where the measured SFDR is plotted as a function of modulation frequency over a range of 0.5–10 GHz, both for 1-MHz noise bandwidth and normalized to 1 Hz. A 120-μm-long device was here used to provide sufficient bandwidth.

Also shown in Fig.16 is the combined effect of RINand shot noise of the laser. It is seen that the frequency-dependent variation of the measured SFDR can be explained down to less than 2 dB margin by the RIN level, indicating relatively frequency-independent linearity behavior of the EAM. Improved SFDR can therefore be achieved by reducing the RIN level at higher frequencies by increasing gain section bias, as indicated by Fig. 3. However, to do this, the power handling of the device will need to be improved to accommodate the increased Joule heating. At all frequencies, the third-order distortion products could be suppressed to a level such that the subharmonic SFDR was limited by fifth-order distortion products. The EAM bias point needed to achieve this varied in a $-2.95 + / - 0.1$ V range. The cause for this variation of bias point was residual distortion from the RF sources, even though care was taken to reduce the residual relative distortion to a level suppressed by at least 15 dB relative to that of the modulator. The magnitude of the distortion of the EAM was insensitive to the residual distortion of the RF sources.

VI. LINK PERFORMANCE

The integrated SGDBR-SOA-EAM device was applied as the optical transmitter in an analog link experiment. Microwave-to-optical conversion was achieved by modulating an unmatched EAM, while a 50-Ω back-terminated 0.8 A/W Discovery photodetector was used for optical-to-microwave conversion. Fig. 17 shows the resulting link gain and noise figure as a function of EAM bias at $\lambda = 1552$ nm and 1-GHz modulation frequency. The link gain peaks at -20.7 dB between -1.4 and -1.5 V EAM bias voltage. The gain can be somewhat improved by removing the back-termination of the detector, improving the gain by 6 dB gain, or using a high-impedance receiver circuit. Reducing the transmitter fiber coupling loss will improve the gain further. However, ultimately to achieve optical link gain, the limitations imposed by the EAM photocurrent need to be addressed. Using the limit derived for maximum conversion efficiency of an EAM,
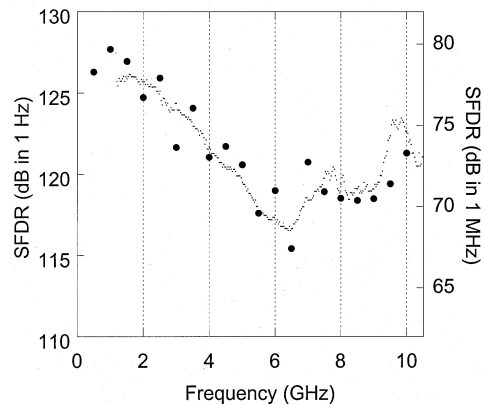

Fig. 16. Measured EAM SFDR versus modulation frequency for 1-MHz bandwidth and normalized to 1 Hz at $\lambda = 1554$ nm (large circles). Also shown (small circles) is relative effect on SFDR from the RIN level of the source.
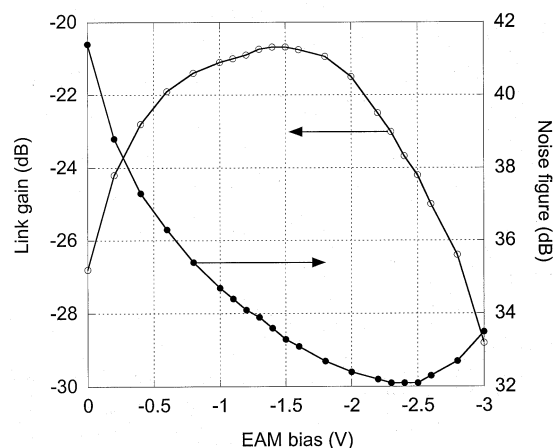

Fig. 17. Link gain and noise figure as a function of EAM bias voltage at $\lambda = 1552$ nm for 180-mA gain section bias and 180-mA SOA bias.

derived in the last section, increasing the optical power will only improve the link gain by a maximum 4.6 dB, limiting the available gain of the link in the current configuration to -16.1 dB.

The link noise figure reaches its lowest level at a voltage different from where the link gain peaks. The reason for this is found in the RIN limited noise characteristic of the link. While the decreasing average output optical power at lower EAM bias will not change the level of the noise floor relative to optical power, the relative slope sensitivity will increase and so will then the modulated signal level, normalized by average transmitted power. There exists an optimum EAM bias for minimum noise figure where the improvements in relative slope sensitivity and the onset of shot-noise-limited noise performance balances out—in this case at -2.4 V, resulting in a noise figure of 32.1 dB. This phenomenon has been referred to as "low biasing" the external modulator and has been observed using well-balanced Mach–Zehnder modulators [23]. Fig. 18 shows the link gain and noise figure as a function of applied SOA bias, again at λ=1552 nm and 1-GHz modulation frequency, with the EAM being biased at maximum slope sensitivity. As expected, the link gain increases with SOA bias and optical
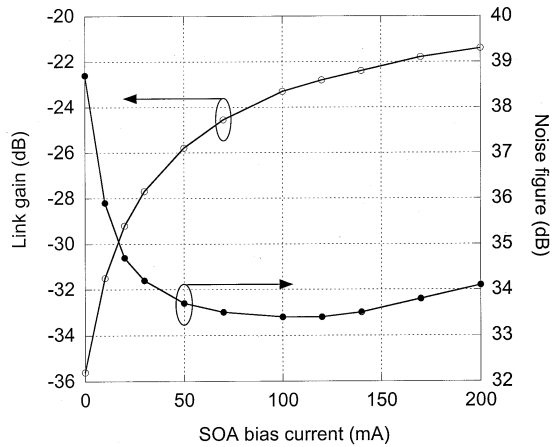
Fig. 18. Link gain and noise figure as a function of SOA bias current at $\lambda = 1552$ nm for 180-mA gain section bias and -1.4-V EAM bias.

power. The noise figure reaches a minimum level between 100 to 120mA. Compared tothe measured RIN performance versus SOA bias, shown in Fig. 4, the best noise performance is slightly shifted to lower values of SOA bias current. This can be attributed to additional heating of the device from the absorbed EAM photocurrent.

VII. CONCLUSION

The performance of sampled-grating DBR laser-based integrated optical transmitters has been characterized for analog applications. An SGDBR laser, integrated to an SOA and an EAM, has a tuning range greater than 45 nm, with more than 40-dB sidemode suppression ratio. The peak RIN is lower than -153 dB/Hz for higher bias currents to the SOA and gain sections. The gain of the SOA of the integrated device results in an equivalent 370% modulation conversion efficiency. Two approaches to enhance the direct modulation performance of SGDBR lasers are summarized: the use of gain-levered SGDBR lasers and inclusion of multiple series-connected gain sections.

For devices integrated to an electroabsorption modulator, the response was found to be determined by the absorbed photocurrent, in terms of bandwidth and conversion efficiency, and in that self-matching to a 50-Ω impedance was observed at low frequencies and typical optical operating power. The suboctave SFDR of the EAM is between 125–127 dB $\cdot$ Hz$^{4/5}$ over the wavelength range, and the broadband SFDR is in the range 103–107 dB $\cdot$ Hz$^{2/3}$, limited by third-order intermodulation products or 95–98 dB $\cdot$ Hz$^{1/2}$, limited by second-order intermodulation products. Applied in an analog link experiment, a link gain of -20.7 dB with a corresponding noise figure of 33.3 dB was found. However, by low-biasing the modulator, the link noise figure could be reduced to - 32.1 dB at the expense of lower gain. In terms of link performance, the link gain will be significantly improved by decreasing optical coupling losses and increasing receiver sensitivity. However, to achieve a low noise figure, or come close to zero link loss, the modulator response must ultimately be much improved. For absorptive modulators, the degradation of modulation sensitivity due to absorbed photocurrent must be overcome. Interferometric mod-

ulators, such as the Mach–Zehnder modulator, do not have this limitation. Integration of SGDBR lasers to a Mach–Zehnder modulator is currently under investigation [24].

REFERENCES

[1] K. Noguchi, O. Mitomi, and O. Miyazawa, "Millimeter-wave Ti : LiNbO$_3$ optical modulators," *IEEE J. Lightwave Technol.*, vol. 16, pp. 615–619, 1998.

[2] C. Cox, H. Roussell, R. Ram, and R. Helkey, "Broadband, directly modulated analog fiber optic link with positive intrinsic gain and reduced noise figure," in *Proc. IEEE Int. Topical Meeting Microwave Photonics*, Princeton, NJ, 1998.

[3] W. K. Burns, M. M. Howerton, and R. P. Moeller, "Broad-band unamplified optical link with RF gain using a LiNbO$_3$ modulator," *IEEE Photon. Technol. Lett.*, vol. 11, pp. 1656–1658, Dec. 1999.

[4] E. Ackerman, C. Cox, G. Betts, H. Roussell, K. Ray, and F. O'Donnell, "Input impedance conditions for minimizing the noise figure of an analog optical link," *IEEE Trans. Microwave Theory Tech.*, vol. 46, pp. 2025–2031, Dec. 1998.

[5] G. Betts, "Linearized modulator for suboctave-bandpass optical analog links," *IEEE Trans. Microwave Theory Tech.*, vol. 42, pp. 2642–2649, Dec. 1994.

[6] Y. A. Akulova, G. A. Fish, P. C. Koh, C. Schow, P. Kozodoy, A. Dahl, S. Nakagawa, M. Larson, M. Mack, T. Strand, C. Coldren, E. Hegblom, S. Penniman, T. Wipiejewski, and L. A. Coldren, "Widely-tunable electroabsorption-modulated sampled grating DBR laser transmitter," *IEEE J. Select. Topics Quantum Electron.*, vol. 8, pp. 1349–1357, Nov./Dec. 2002.

[7] V. Jayaraman, Z.-M. Chuang, and L. A. Coldren, "Theory, design, and performance of extended tuning range semiconductor laser with sampled grating," *IEEE J. Quantum Electron.*, vol. 29, pp. 1824–1834, 1993.

[8] B. Mason, G. A. Fish, S. P. DenBaars, and L. A. Coldren, "Widely tunable sampled grating DBR laser with integrated electroabsorption modulator," *IEEE Photon. Technol. Lett.*, vol. 11, pp. 638–640, 1999.

[9] H.Hanxing Shi, D. Cohen, J. Barton, M. Majewski, L. A. Coldren, M. C. Larson, and G. A. Fish, "Relative intensity noise measurements of a widely tunable sampled-grating DBR laser," *IEEE Photon. Technol. Lett.*, vol. 14, pp. 759–761, Jun 2002.

[10] M. L. Majewski, J. Barton, L. A. Coldren, Y. Akulova, and M. C. Larson, "Direct intensity modulation in sampled-grating DBR lasers," *IEEE Photon. Technol. Lett.*, vol. 14, pp. 747–749, June 2002.

[11] M.L. Majewski, "Widely tunable directly modulated sampled-grating DBR lasers," in *Proc. OFC 2002*, paper ThV2.

[12] H. X. Shi, D. A. Cohen, J. Barton, M. Majewski, L. A. Coldren, M. C. Larson, and G. A. Fish, "Dynamic range of widely tunable sampled grating DBR lasers," *Electron. Lett.*, vol. 38, pp. 180–181, 2002.

[13] K. Vahala, M. Newkirk, and T. Chen, "The optical gain lever: a novel gain mechanism in the direct modulation of quantum well semiconductor lasers," *Appl. Phys. Lett.*, vol. 54, pp. 2506–2508, 1989.

[14] C. P. Seltzer, L. D. Westbrook, and H. J. Wickes, "Improved signal-to-noise ratio in gain-levered InGaAs/InP MQW lasers," *Electron. Lett.*, vol. 29, pp. 230–231, 1993.

[15] L. D. Westbrook and C. P. Seltzer, "Reduced intermodulation-free dynamic range in gain-lever lasers," *Electron. Lett.*, vol. 29, pp. 488–489, 1993.

[16] K. D. Choquette, E. Young, K. Geib, D. Serkland, A. Allerman, C. Cox, E. Ackerman, and H. Roussell, "Cascade vertical cavity surface emitting laser arrays," in *2002 IEEE/LEOS Annu. Meeting Conf. Proc.*, 2002, paper TuAA1, pp. 327–328.

[17] J. Getty, E. Skogen, and L. A. Coldren, "Segmented 1.55 um laser with 400% differential quantum efficiency," in *Proc. OFC 2003*, paper TuG1.

[18] R. Ludwig and A. Ehrhardt, "Turn-key-ready wavelength-, repetition rate- and pulsewidth-tunable femtosecond hybrid modelocked semiconductor laser," *Electron. Lett.*, vol. 31, pp. 1165–1167, 1995.

[19] G. L. Li, P. K. L. Yu, W. S. C. Chang, K. K. Loi, C. K. Sun, and S. A. Pappert, "Concise RF equivalent circuit model for electroabsorption modulators," *Electron. Lett.*, vol. 36, pp. 818–820, 2000.

[20] M. S. Islam, S. Murthy, T. Itoh, M. C. Wu, D. Novak, R. B. Waterhouse, D. L. Sivco, and A. Y. Cho, "Velocity-matched distributed photodetectors and balanced photodetectors with p-i-n photodiodes," *IEEE Trans. Microwave Theory Tech.*, vol. 10, pp. 1914–1920, Oct 2001.

[21] T. H. Wood, J. Z. Pastalan, C. A. Burrus Jr, B. C. Johnson, B. I. Miller, J. L. deMiguel, U. Koren, and M. G. Young, "Electric field screening by photogenerated holes in multiple quantum wells: a new mechanism for absorption saturation," *Appl. Phys. Lett.*, vol. 57, pp. 1081–1083, 1990.

[22] L. A. Johansson, Y. A. Akulova, G. A. Fish, and L. A. Coldren, "High optical power electroabsorption waveguide modulator," *Electron. Lett.*, vol. 39, pp. 364–365, 2003.

[23] M. Farwell, W. Chang, and D. Huber, "Increased linear dynamic range by low biasing the Mach-Zehnder modulator," *IEEE Photon. Technol. Lett.*, vol. 5, pp. 779–782, July 1993.

[24] J. S. Barton, E. J. Skogen, M. L. Masanovic, S. P. DenBaars, and L. A. Coldren, "Tailorable chirp using integrated Mach-Zehnder modulators with tunable sampled grating distributed Bragg reflector lasers," in *IEEE 18th Int. Semiconductor Laser Conf.*, 2002, pp. 49–50.